J|A|C|S
ARTICLES
Published on Web 07/04/2002

Structural Characterization, Optical Properties, and Improved Solubility of Carbon Nanotubes Functionalized with Wilkinson's Catalyst

Sarbajit Banerjee[†] and Stanislaus S. Wong*[,†,‡]

Contribution from the Department of Chemistry, State University of New York at Stony Brook, Stony Brook, New York 11794, and Materials and Chemical Sciences Department, Brookhaven National Laboratory, Building 480, Upton, New York 11973

Received April 10, 2002

Abstract: Oxidized carbon nanotubes have been reacted with Wilkinson's complex. It has been found that the Rh metal coordinates to these nanotubes through the increased number of oxygen atoms, forming a hexacoordinate structure around the Rh atom. The reaction process increases oxidized nanotube solubility in DMSO (>150 mg/L) as well as to a certain extent in DMF and THF. The functionalization process results in exfoliation of larger bundles of SWNTs and may select for the presence of distributions of smaller-diameter tubes. Optical data on the derivatized adducts suggest the possibility of interesting charge-transfer behavior across the metal−nanotube interface. An application has been made of this system as supports for homogeneous catalysis.

Introduction

Single-walled carbon nanotubes (SWNTs)[1] have been extensively studied over the past few years due to their unique and desirable structure-dependent[2] mechanical, electrical, and electromechanical properties.[3,4] Recently, the chemical derivatization of carbon nanotubes has attracted a lot of attention and effort, since understanding the molecular basis for functionalization has implications for composite formation, photophysical analysis, and rational self-assembly of these nanostructures. Moreover, controlled chemical functionalization has the potential to impact research in catalysis[5] as well as in molecular electronics.[6] Several derivatization approaches have been tried including electrochemical reduction[7] of aryl diazonium salts, 1,3 dipolar cycloaddition of azomethine ylides,[8] noncovalent attachment through a bifunctional molecule,1-pyrenebutanoic acid, succinimdyl ester irreversibly adsorbed onto the hydrophobic surfaces of the tubes in DMF,[9] fluorination by means of elemental fluorine,[10] and ultrasonication in a monochlorobenzene solution of poly(methyl methacrylate).[11]

Solubilization of tubes through functionalization is also a key objective.[12] It has been proposed that large organic groups assist in solubility by exfoliation of the bundles into individual tubes through the formation of intervening moieties that can overcome the intrinsic van der Waals forces[7] between these tubes. An alternative strategy that we have been exploring is to derivatize SWNTs with relatively bulky inorganic complexes, which not only yields a novel metal-based molecular coordination complex but also offers the possibility of tailorable solubility in a variety of solvents through mechanisms such as charge-mediated stabilization along the length of the tube, without completely disrupting the tube's electronic structure. In addition, these generated adducts can be used in a number of different catalytic processes, including homogeneous catalysis, upon which the expensive metal−support assembly can be facilely recovered from solution.

In previous work, we have demonstrated that Ir metal, in the form of Vaska's complex, can coordinate to raw and oxidized SWNTs through two distinctive pathways. In effect, with raw tubes, the process happens through an η^2-coordination process, while with oxidized tubes, the reaction occurs through the increased density of oxygen atoms, forming a hexacoordinate structure around the Ir atom.[5] Herein, we describe the synthesis and systematic characterization of the properties of an adduct of SWNTs, derivatized with another metal complex of importance to inorganic and organometallic chemistry,

* To whom correspondence should be addressed. Telephone: 631-632-1703. Fax: 631-344-3178. E-mail: sswong@ms.cc.sunysb.edu; sswong@bnl.gov.
† SUNY at Stony Brook.
‡ Brookhaven National Laboratory.

(1) Thess, A.; Lee, R.; Nikolaev, P.; Dai, H.; Petit, P.; Robert, J.; Xu, C.; Lee, Y. H.; Kim, S. G.; Rinzler, A. G.; Colbert, D. T.; Scuseria, G. E.; Tomanek, D.; Fischer, J. E.; Smalley, R. E. *Science* **1996**, *273*, 483.
(2) Dresselhaus, M. S.; Dresselhaus, G.; Eklund, P. C. *Science of Fullerenes and Carbon Nanotubes*; Academic Press: New York, 1996.
(3) Falvo, M. R.; Clary, G. J.; Taylor, R. M. I.; Chi, V.; Brooks, F. P. J.; Washburn, S.; Superfine, R. *Nature* **1997**, *389*, 582.
(4) Odom, T. W.; Huang, J.-L.; Kim, P.; Lieber, C. M. *Nature* **1998**, *391*, 62.
(5) Banerjee, S.; Wong, S. S. *Nano Lett.* **2002**, *2*, 49.
(6) Banerjee, S.; Wong, S. S. *Nano Lett.* **2002**, *2*, 195.
(7) Bahr, J. L.; Yang, J.; Kosnynkin, V.; Bronikowski, M. J.; Smalley, R. E.; Tour, J. M. *J. Am. Chem. Soc.* **2001**, *123*, 6536.
(8) Georgakilas, V.; Kordatos, K.; Prato, M.; Guldi, D. M.; Holzinger, M.; Hirsch, A. *J. Am. Chem. Soc.* **2002**, *124*, 760.
(9) Chen, R. J.; Zhang, Y.; Wang, D.; Dai, H. *J. Am. Chem. Soc.* **2001**, *123*, 3838.
(10) Mickelson, E. T.; Huffman, C. B.; Rinzler, A. G.; Smalley, R. E.; Hauge, R. H.; Margrave, J. L. *Chem. Phys. Lett.* **1998**, *296*, 188.
(11) Koshio, A.; Yudasaka, M.; Zhang, M.; Iijima, S. *Nano Lett.* **2001**, *7*, 361.
(12) Chen, J.; Hamon, M. A.; Hu, H.; Chen, Y.; Rao, A. M.; Eklund, P. C.; Haddon, R. C. *Science* **1998**, *282*, 95.

10.1021/ja026487o CCC: $22.00

namely the catalytically significant Wilkinson's compound, $RhCl(PPh_3)_3$, alternatively known as tris-triphenylphosphine rhodium(I) chloride.

The adduct has been characterized by a number of different methodologies, including ^1H, ^{13}C, and ^{31}P NMR spectroscopy; X-ray diffraction (XRD); transmission electron microscopy (TEM); scanning electron microscopy (SEM); atomic force microscopy (AFM); as well as energy-dispersive X-ray spectroscopy (EDAX). Spectroscopically, UV−visible, near-infrared (NIR), and luminescence data have been collected. In terms of solubility, it has been found that low concentrations of Wilkinson's complex are sufficient to dissolve large amounts of the SWNT material. The adduct also shows a comparatively high degree of solubility in DMSO, reproducibly >150 mg/L, and up to as much as 250 mg/L. Reasonable solubility values (roughly 30% of that noted in DMSO) of functionalized tubes have been noted in DMF and THF, which are generally considered to be poor-to-moderate solvents for underivatized SWNTs.[13,14] The values for unfunctionalized but oxidized tubes are in the range of 7−15 mg/L and 4−10 mg/L for DMF and THF, respectively.

Experimental Section

Nanotube Synthesis and Purification. Raw SWNTs (Figure 1a) were produced by the laser oven method (Carbolex, Lexington, KY), and individual tubes have a reported mean diameter of 1.41 nm, although experimentally, a large distribution of diameters was observed. The raw SWNT material contains about 30 wt % of metal catalysts, such as Ni and Co. To purify these materials, the SWNTs were oxidized according to existing procedures by an acidic $KMnO_4$ solution[15] and then washed thoroughly with HCl and water. Carboxylic acid groups are expected to be the predominant species on the opened caps and defect sites. SEM (Figure 1a) and TEM (Figure 1, b and c) results showed that the oxidation process not only removed most of the amorphous carbon but also the majority of the metal particles; furthermore, X-ray diffraction data (Figure 2, inset) indicated the disappearance of the catalyst-related (100) and (200) peaks of cubic Ni and Co for posttreated tubes. The purified tubes were then dried at 100 °C and redispersed in DMSO by mild sonication (20 s).

Generally, solvents, such as dimethylformamide and tetrahydrofuran (Acros Fisher), were used after distillation and were stored over 4 Å molecular sieves. All other reagents were obtained commercially and used without further purification.

Synthesis of SWNT−Wilkinson's Adduct. In a typical synthesis, the reaction was carried out in a Schlenk setup. To a briefly sonicated nanotube dispersion in DMSO was added, dropwise, 10 mL of a 10 mM solution of Wilkinson's catalyst in DMSO solution under vigorous stirring, in an inert Ar atmosphere. The reaction mixture was then stirred at 55−60 °C for a period of 80 h. It was observed that a substantial portion of the nanotubes dissolve into a visually, nonscattering solution. The reaction mixture was filtered over a 0.2-μm Nylon membrane, after which undispersed chunks of unreacted bucky paper were removed, and the remaining solid was then successively washed with DMSO, ethanol, and water.

The dissolved tubes in solution could be salted or precipitated out by adding in a saturated aqueous NaCl solution. These were purified by filtering over a 0.2-μm Nylon membrane and washing in an analogous manner as previously described. In terms of solubility behavior, the synthesized adducts could be readily redissolved in DMSO by mild stirring, demonstrating the reversibility of the dissolution process, and the resultant product was stable, even after four months. The product is not particularly air-sensitive, but if left out in the ambient atmosphere for extended periods of time, oxidation of some of the triphenylphosphine groups to triphenylphosphine oxide is inevitable. Dissolution of the adducts in THF and DMF was also observed, but the derivatized tubes tended to precipitate out of solution within a day.

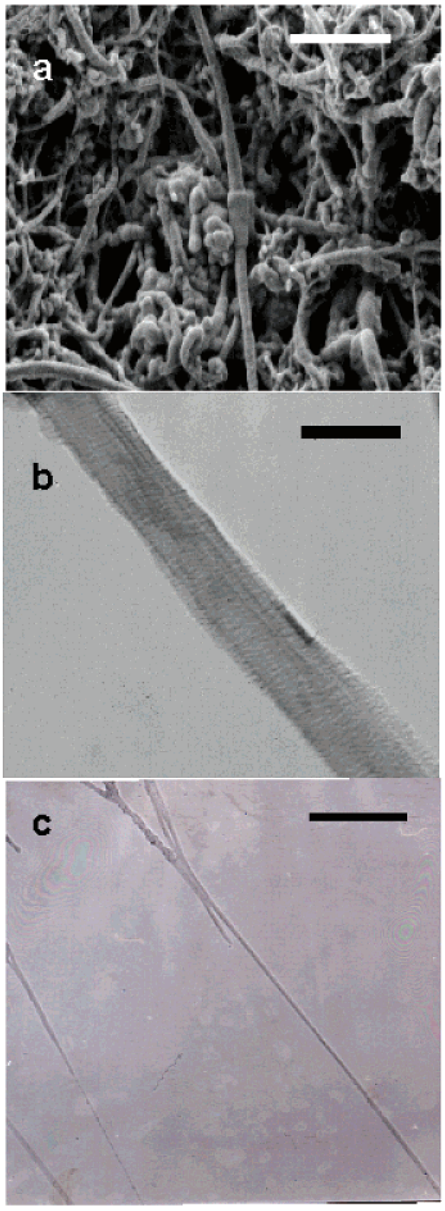

Figure 1. (a) Scanning electron micrograph (SEM) of unpurified, pristine nanotube bundles. Scale bar represents 700 nm. (b) TEM of a purified single-walled carbon nanotube bundle. The scale bar denotes 30 nm. (c) TEM image showing exfoliation of nanotubes (functionalized with Wilkinson's complex) into smaller bundles and individual tubes. Scale bar is 30 nm.

Catalysis with SWNT−Wilkinson's Adduct. The adduct-mediated hydrogenation reaction of cyclohexene was carried out in a DMSO/$CHCl_3$ mixed solvent system by bubbling in a mixture of hydrogen gas in argon under Schlenk conditions for a period of 3 days at room temperature. Typically, 1 mL of a saturated solution of the supported catalyst in DMSO was stirred with 3 mL of $CHCl_3$ and 3 mL of cyclohexene. The reaction was monitored by ^1H NMR spectroscopy through the appearance of cyclohexane peaks at ~1.52 ppm. The reaction yield obtained was approximately 30%, but it is expected that

(13) Bahr, J. L.; Mickelson, E. T.; Bronikowski, M. J.; Smalley, R. E.; Tour, J. M. *Chem. Commun.* **2001**, *2001*, 193.
(14) Ausman, K. D.; Piner, R.; Lourie, O.; Ruoff, R. S.; Korobov, M. *J. Phys. Chem. B* **2000**, *104*, 8911.
(15) Hiura, H.; Ebbesen, T. W.; Tanigaki, K. *Adv. Mater.* **1995**, *7*, 275.

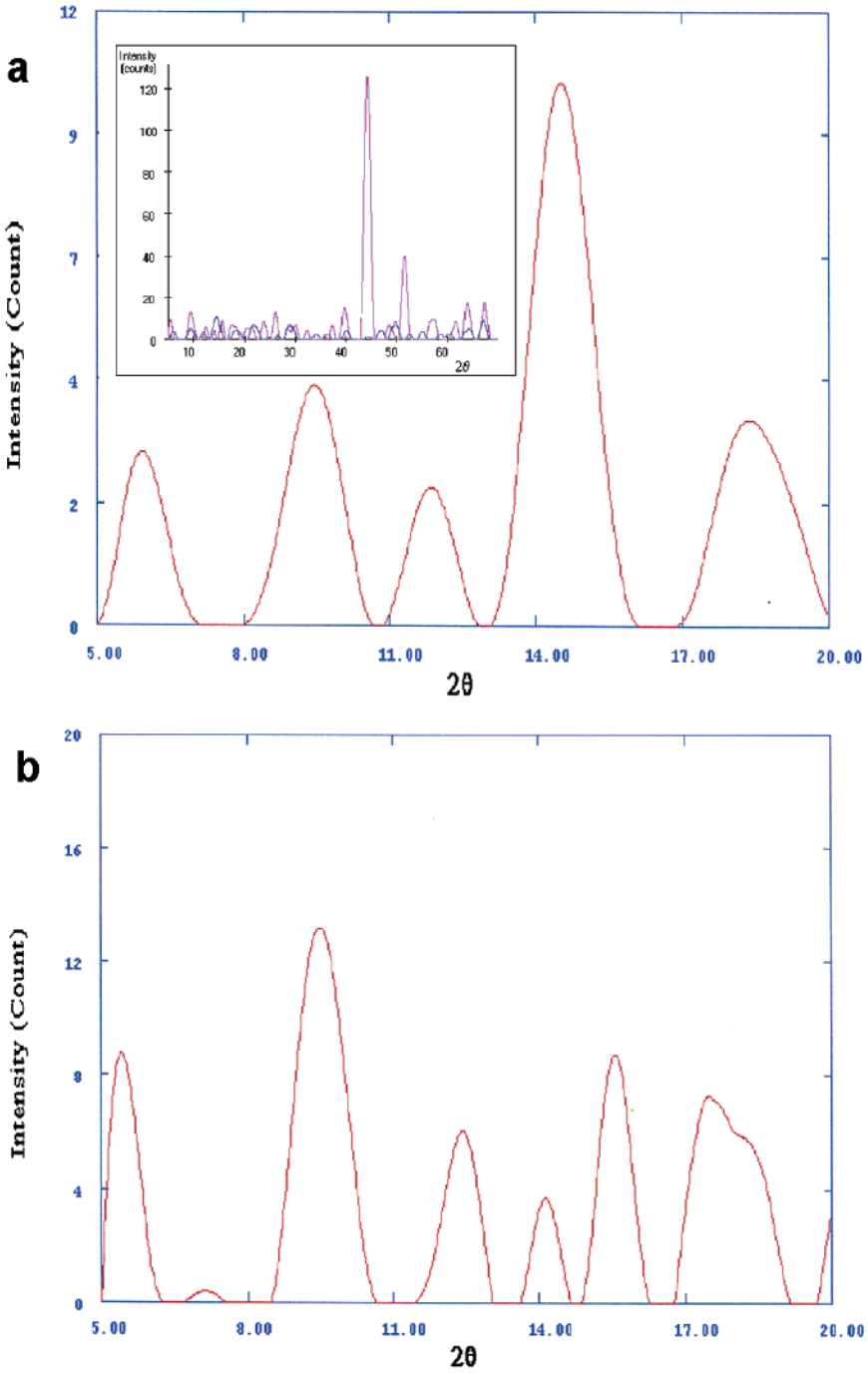

Figure 2. Selected regions of background subtracted powder X-ray diffraction spectra of (a) functionalized nanotubes and (b) as prepared raw nanotubes from 2θ values of 5−20°. The reflections can be indexed to a two-dimensional triangular lattice. The *10* peak is shifted from 2θ ∼5.43° (raw tubes) to 2θ ∼5.92° upon derivatization. Broadening of the peak is also observed. The inset shows the entire diffraction spectra for 2θ values of 5−70° for raw tubes (pink) and functionalized nanotube adducts (blue), respectively. The Ni−Co (100) and (200) peaks are absent in the functionalized sample. The retention of lattice peaks indicates that the tubes are able to assemble as bundles on solvent removal.

a higher yield is likely with further optimization of the solvent system and with an improved hydrogenation apparatus.

Electron Microscopy. Samples for TEM were obtained by drying sample droplets from an ethanolic or DMSO solution onto a 300 mesh Cu grid with a lacey carbon film. All the micrographs were taken at an accelerating voltage of 120 kV on a Philips CM12 TEM, equipped with EDAX capabilities. SEM images were obtained on Cu grids as well at accelerating voltages of 1−2 kV at a 2-mm working distance using a Leo 1550 field emission instrument.

Atomic Force Microscopy. AFM height images were taken in Tapping mode in air at resonant frequencies of 50−75 kHz with oscillating amplitudes of 10−100 nm. The samples were spin coated onto a mica substrate, and imaged with Si tips (k = 1−5 N/m) using a Multimode Nanoscope IIIa (Digital Instruments, Santa Barbara, CA).

Nuclear Magnetic Resonance. Deuterated solvents, including $CDCl_3$, d_6-DMF, d_6-DMSO, and d_7-THF, were purchased from Aldrich and used without further purification. All NMR spectra were obtained on a Bruker AC-250 multinuclear FT-NMR at 298 K. The ^{31}P and ^{13}C NMR data were proton decoupled.^{31}P NMR results are referenced to an external phosphoric acid standard.

X-ray Diffraction. Powder X-ray diffraction spectra were collected on a Scintag diffractometer, operating in the Bragg configuration using

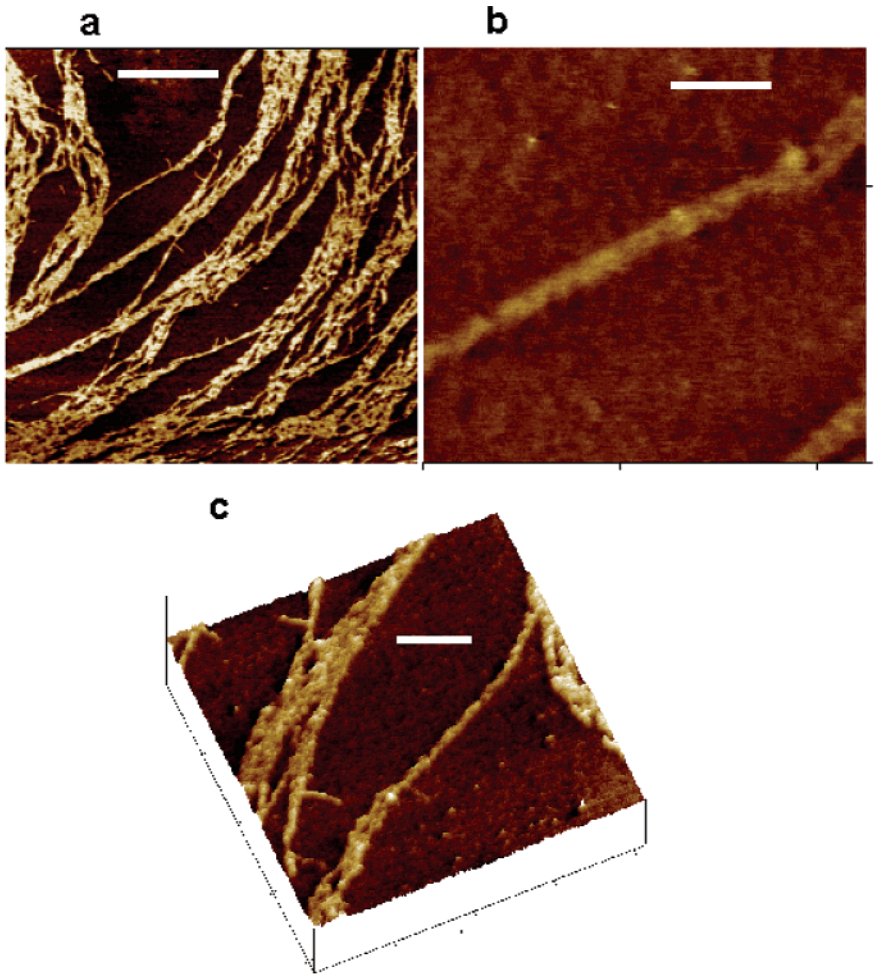

Figure 3. Atomic force microscopy (AFM) height images of functionalized nanotube adducts. Scale bars are (a) 500 nm, (b) 100 nm, and (c) 200 nm. (a) A high density of tubes has been deposited from solution. Aggregates of tubes appear to be exfoliating into smaller bundles. (b) Image of a single bundle, approximately 15 nm in diameter. (c) A 3-D view of exfoliating tubes. The bundles and tubes are relatively clean and free of nanoparticulate matter

Cu Kα radiation ($\lambda = 1.54$ Å). A Soonerveld background subtraction was performed to remove low Q diffuse reflections. Parameters used for slit widths and accelerating voltage, as well as Savitzky−Golay smoothing algorithms, were identical for all the samples.

Optical Spectroscopy. UV spectra were obtained at high resolution on a ThermoSpectronics UV1 using quartz cells with a 10-mm path length. NIR spectra were obtained on a Nicolet Nexus 670 spectrophotometer with a CaF_2 beam splitter and an InGaAs room-temperature detector using a 5-mm path length quartz cell. All spectra collected were corrected to account for a background of the appropriate solvent. Fluorescence data were obtained on a Jobin Yvon Spex Fluorolog 3.22, equipped with a 450-W xenon source and configured with double monochromators for both emission and excitation, with a 1-s integration time, to provide for stray light rejection while maintaining high light throughput. The experiments were performed using front face collection optics to collect the emission most efficiently.

Results and Discussion

Microscopy. Electron microscopy (Figure 1) and AFM data (Figure 3) of the derivatized adducts indicate a high density of small bundles, of the order of 15−20 nm in diameter (as compared with 30 nm on average for unfunctionalized tubes) and up to a few micrometers in length, as well as individual tubes, arising from exfoliation of larger bundles. The high purity of the purified starting material and the relatively large abundance of predominantly clean nanotubes, relatively free of particulate impurities, in SEM and TEM images of the synthesized adduct indicates that it is indeed the SWNTs, and not other extraneous impurities, that have been derivatized and dissolved. EDAX data confirm the presence of Rh, P, and Cl elemental signatures on the functionalized tubes, with less than 1% loading of the functional moieties.

It is predicted that molecules of the bulky inorganic complex, spread along the length of the SWNT, lead to disruption of the intertube interactions and thereby enable these small tubular bundles to stay apart in solution in an analogous manner in which bulky organic groups and polymers do so.[16−18] The fact that the tubes can be precipitated out upon the addition of a high-ionic strength solution suggests that the tubes are charged to some extent in solution and that solubility observed occurs by means of electric double-layer stabilization. The presence of charge likely originates in carboxylate anion-like species, formed during the purification procedure, coordinating to the Rh center of Wilkinson's complex.

(16) Bandyopadhayaya, R.; Nativ-Roth, E.; Regev, O.; Yerushalmi-Rozen, R. *Nano Lett.* **2002**, *2*, 25.
(17) Chen, J.; Rao, A. M.; Lyuksyutov, S.; Itkis, M. E.; Hamon, M. A.; Hu, H.; Cohn, R. W.; Eklund, P. C.; Colbert, D. T.; Smalley, R. E.; Haddon, R. C. *J. Phys. Chem. B* **2001**, *105*, 2525.
(18) O'Connell, M. J.; Boul, P.; Ericson, L. M.; Huffman, C.; Wang, Y.; Haroz, E.; Kuper, C.; Tour, J.; Ausman, K. D.; Smalley, R. E. *Chem. Phys. Lett.* **2001**, *342*, 265.

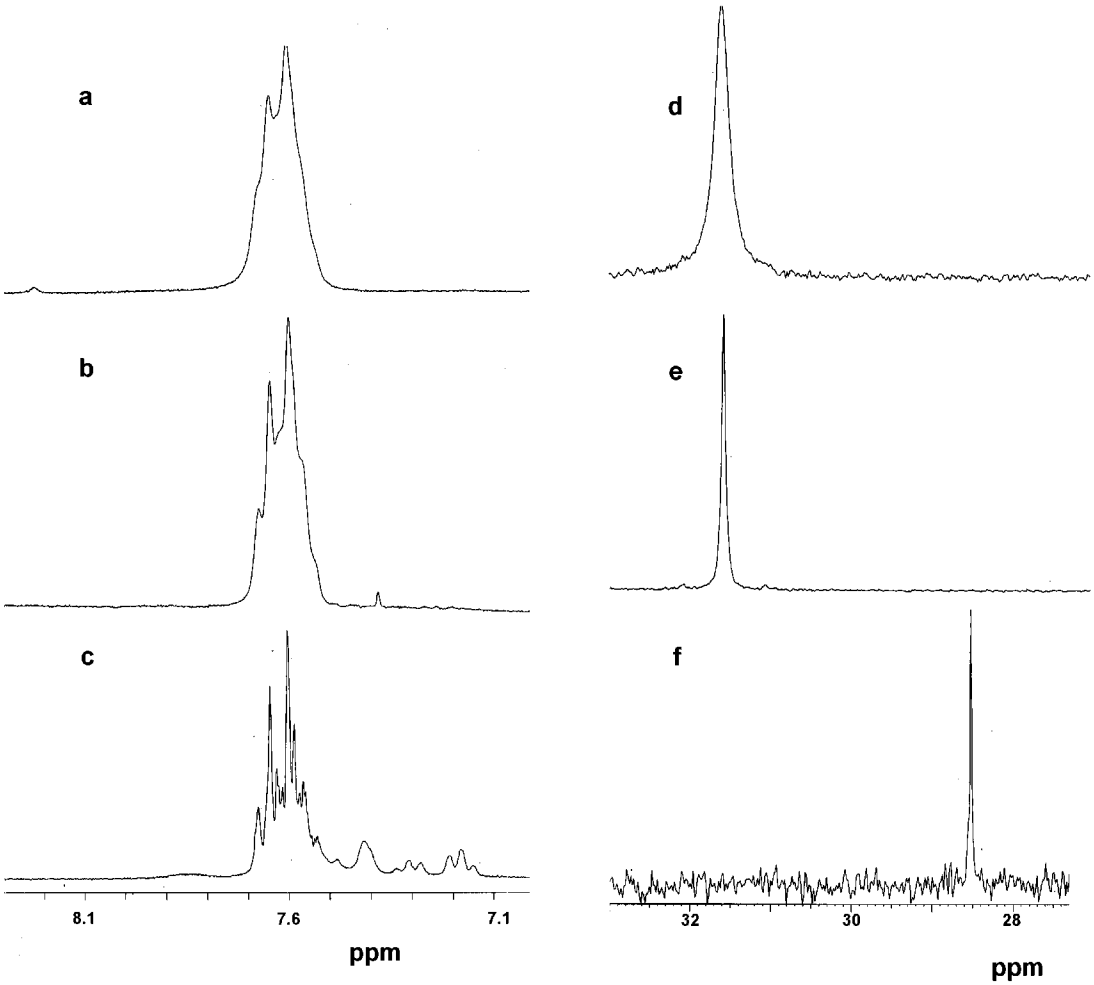

Figure 4. ^{1}H and ^{31}P NMR spectra of functionalized nanotubes at different concentrations and controls. Parts (a−c) are ^{1}H NMR spectra, while parts (d−f) are ^{31}P NMR spectra. All spectra have been taken in d_6-DMSO at 298 K. (a) A saturated solution of SWNT−Wilkinson's compound adduct. (b) A 40% dilution of the saturated nanotube−Wilkinson's adduct solution from (a). (c). Wilkinson's compound, $Rh(PPh_3)_3Cl$. (d−f) are the corresponding ^{31}P NMR spectra for solutions (a−c), respectively.

X-ray Diffraction. The powder XRD pattern for a solid, functionalized adduct sample shows recovery of the nanotube lattice peaks (Figure 2a), indicating that the tubes are able to coalesce together upon solvent removal. The relative broadness of the *10* peak (Figure 2a), though, with respect to the initial Carbolex peaks (Figure 2b), is consistent with the presence of lattice mismatch induced by chemical derivatization,[19] and moreover, this peak also shows a shift toward higher *q*. The powder profile and the position of the *10* reflection is sensitive to a number of parameters including the size of the bundle, the tube diameter, the distribution of these tube diameters, and the lattice constant.[20−22] Hence, the broadened peak observed can be accounted for by a smaller aggregate tube bundle size,[22] whereas the upshift in *q* values can be explained by the presence of a larger quantity of smaller-diameter tubes within the functionalized adduct sample as compared with that of the original raw SWNT sample. A smaller tube bundle size would also be consistent with the presence of exfoliation in solution, as suggested by the microscopy data.

NMR Spectroscopy. NMR spectroscopy confirmed the coordination of the complex onto the oxidized tubes. In particular, ^{31}P, ^{1}H, and ^{13}C NMR spectra of the adduct were obtained. Comparison of the ^{31}P and ^{1}H NMR data with that of the starting material, $RhCl(PPh_3)_3$, is shown in Figure 4. Figure 4, a and d, represents data corresponding to saturated solutions of nanotube−adduct complexes, whereas Figure 4, b and e, is associated with results at 40% saturation. There are two important features observed in all of these spectra. First, there is a chemical shift difference of ∼3 ppm in the ^{31}P NMR data between the resonances of the adduct and of Wilkinson's catalyst, consistent with the formation of a derivatized product.[23] Thus, the relatively small chemical shift changes observed from the starting material to the adduct are evidence of coordination of the Rh metal center to oxygen atoms on the tube as opposed to through direct involvement of the phosphine ligands.

Second, as noted with other types of functionalizations performed, the NMR peaks of nanotubes tend to broaden upon derivatization.[18,24] In this work, we postulate that since the large nanotubes move relatively slowly on the NMR time scale of

(19) Maurin, G.; Stepanek, I.; Bernier, P.; Colomer, J.-F.; Nagy, J. B.; Henn, F. *Carbon* **2001**, *39*, 1273.
(20) Anglaret, E.; Rols, S.; Sauvajol, J.-L. *Phys. Rev. Lett.* **1998**, *81*, 4780.
(21) Fujiwara, A.; Ishii, K.; Suematsu, H.; Kataura, H.; Maniwa, Y.; Suzuki, S.; Achiba, Y. *Chem. Phys. Lett.* **2001**, *336*, 205.
(22) Rols, S.; Almairac, R.; Henrard, L.; Anglaret, E.; Sauvajol, J.-L. *Eur. Phys. J. B* **1999**, *10*, 263.
(23) Star, A.; Stoddart, J. F.; Steuerman, D.; Diehl, M.; Boukai, A.; Wong, E. W.; Yang, X.; Chung, S.-W.; Choi, H.; Heath, J. R. *Angew. Chem., Int. Ed.* **2001**, *40*, 1721.
(24) Sun, Y.-P.; Huang, W.; Lin, Y.; Fu, K.; Kitaygorodsky, A.; Riddle, L. A.; Yu, Y. J.; Carroll, D. L. *Chem. Mater.* **2001**, *13*, 2864.

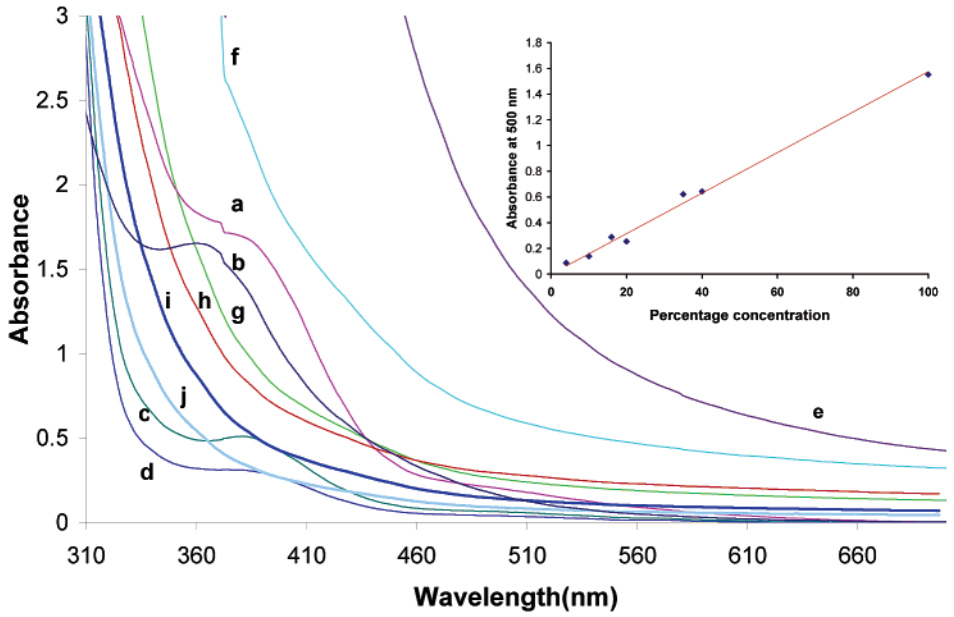

Figure 5. UV−visible electronic spectra of Wilkinson's complex and of functionalized nanotubes, corrected for solvent. (a). Wilkinson's complex in DMSO. (b). Wilkinson's complex in CH_2Cl_2. (c). Wilkinson's complex diluted with 0.1 M PPh_3 in DMSO by a factor of 2. (d). Solution (a) diluted with PPh_3 in DMSO by a factor of 4. (e). Saturated SWNT−Wilkinson's complex adduct solution in DMSO. (f−j). Successive dilutions of solution (e) with either DMSO or 0.1 M PPh_3 in DMSO. Concentration factors are 40, 20, 16, 10, and 4%, respectively. Both types of solvent dilutions yield the same absorbance data in this region of the spectrum. Inset shows a plot of absorbance at 500 nm vs increasing dilution of the functionalized SWNT−Wilkinson's complex adduct solution with either neat DMSO or 0.1 M PPh_3 in DMSO.

measurement, observed broadening of the NMR peaks is indicative of the localization and immobilization, through restriction of the degrees of conformational freedom, of metal complex molecules onto the oxygenated surface sites of the tube with the accompanying loss of symmetry.[25] Indeed, this same broadening trend is observed for all nuclei, including ^{31}P, ^{1}H, and ^{13}C. While inhomogeneities in the local magnetic field induced by the diameter and helicity-dependent diamagnetism of the SWNTs themselves and the partial alignment of the tubes in the magnetic field of the NMR magnet are expected to contribute to peak broadening,[18,26] in our case, the broadening is likely a result not only of slow tumbling and motion of the tubes in solution, preventing rotational averaging, but also of a slow rate of ligand exchange upon complexation to the tubes.

To provide more evidence for the localization mechanism postulated, we note that in pristine Wilkinson's complex, the loss of a triphenylphosphine moiety is facile and indeed a vital step in its catalytic behavior. In DMSO solvent, for the starting material, exchange involving triphenylphosphine takes place very rapidly, such that all the phosphines in the ^{31}P NMR spectra become equivalent (unlike in CH_2Cl_2 or in benzene[27,28]), which is similar to phenomena noted at higher temperatures; also, coupling of the P nucleus to the Rh nucleus is removed. The fact that the phosphine peaks are broadened upon the addition of and reaction with SWNTs suggests the presence of a slower rate of exchange and the inequivalence of the phosphine ligands. Hence, we believe that this phenomenon is steric in nature, arising from reduced accessibility of the metal center for the phosphine ligands due to complexation with the nanotube. Essentially, the nanotube itself can be considered as a bulky, sterically encumbering ligand. Not surprisingly, on increasing the concentration of nanotubes, the ^{1}H NMR spectra, like the ^{31}P NMR data, similarly broaden.

The ^{13}C solution NMR spectrum for the adduct contains broad resonances centered at $\delta = 128.6$, 128.8, 131.4, 131.5, and 132 ppm. DEPT spectra confirmed that all these are C−H aromatic carbons, originating from phosphine groups. No resonances were seen, however, for the nanotube carbons. To the best of our knowledge, nanotube resonances have not as yet been observed in solution NMR studies of these materials,[29] even upon substantial isotopic enrichment with ^{13}C (up to 20 times the natural abundance). Among the reasons cited for this situation include the relatively long relaxation times of nanotube carbons[30] as well as the low concentrations of nanotubes present, even upon saturation, which cannot be readily detected by ^{13}C solution NMR.

Optical Spectroscopy. The UV−visible spectra collected for pure Wilkinson's complex, $RhCl(PPh_3)_3$, in DMSO show evidence of increased peak structure (apparent upon normalization of intensity) with the addition of 0.01 M PPh_3, as the dissociation equilibrium is shifted to monomeric, undissociated species.[31,32] (Figure 5) Its absorbance maximum in DMSO is red-shifted from the literature value[27] of 361 nm in CH_2Cl_2 to 387 nm. The synthesized adduct, however, has a featureless spectrum, indicating that the initial Rh(I) chromophore undergoes reduction during the coordination process. The optical

(25) Holzinger, M.; Vostrowsky, O.; Hirsch, A.; Hennrich, F.; Kappes, M.; Weiss, R.; Jellen, F. *Angew. Chem., Int. Ed.* **2001**, *40*, 4002.
(26) Smith, B. W.; Benes, Z.; Luzzi, D. E.; Fischer, J. E.; Walters, D. A.; Casavant, M. J.; Schmidt, J.; Smalley, R. E. *Appl. Phys. Lett.* **2000**, *77*, 663.
(27) Brown, T. H.; Green, P. J. *J. Am. Chem. Soc.* **1970**, *92*, 2359.
(28) Tolman, C. A.; Meakin, P. Z.; Lindner, D. L.; Jesson, J. P. *J. Am. Chem. Soc.* **1974**, *96*, 2762.
(29) Fu, K.; Huang, W.; Lin, Y.; Riddle, L. A.; Carroll, D. L.; Sun, Y.-P. *Nano Lett.* **2001**, *1*, 439.
(30) Tang, X. P.; Kleinhammes, H.; Shimoda, H.; Fleming, L.; Bennoune, K. Y.; Sinha, S.; Bower, C.; Zhou, O.; Wu, Y. *Science* **2000**, *288*, 492.
(31) Arai, H.; Halpern, J. *Chem. Commun.* **1971**, 1571.
(32) Meakin, P.; Jesson, J. P.; Tolman, C. A. *J. Am. Chem. Soc.* **1972**, *94*, 3240.

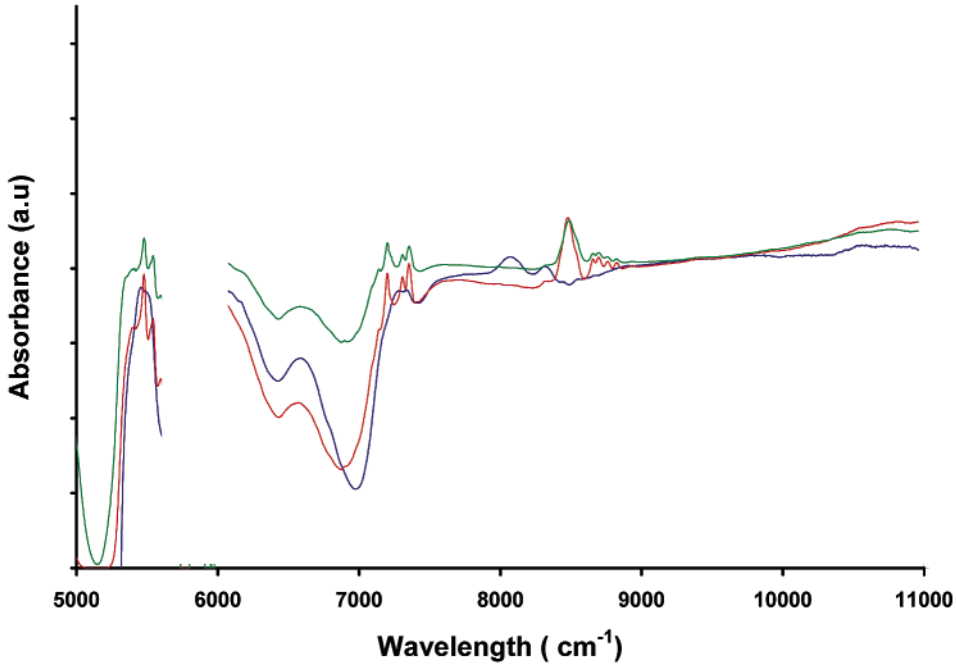

Figure 6. Near-IR spectra of pristine nanotubes (blue) and functionalized SWNT−Wilkinson's complex adduct in DMSO. Spectra of a saturated SWNT−Wilkinson's adduct solution (red) as well as a 40% dilution of this saturated solution (green) are shown. The area of the spectrum omitted consists of high solvent absorbances.

characteristics of the adduct solution, monitored by absorbance at 500 nm, obey Beer's law with respect to relative concentrations; the slope of the linear-least-squares fit is then analogous to an extinction coefficient (Figure 5, inset). The solubility of the tubes was found to be strongly dependent on the concentration of $RhCl(PPh_3)_3$, suggesting that solubilization is chemically induced. Moreover, addition of a large excess of PPh_3 still does not result in the appearance of a λ_{max} feature in the electronic spectrum, indicating that the adduct is probably a Rh (III) species.[32]

The featureless absorbance spectrum of the adduct may correspond to the presence of a large number of absorbing and emitting species, as has been postulated from prior luminescence studies[33] of nanotubes. Indeed, a large number of chromophores would account for the absence of any clear isosbestic points in the electronic spectra. The adduct is, in fact, fluorescent; the strong fluorescence prevented any detection of a Raman signal at 752-nm laser excitation, despite repeated efforts.

Rh complexes are known to have charge-transfer transitions at higher energies; however, interference from solvent DMSO lower than 300 nm makes monitoring these transitions an unreliable task. The DMSO solution of derivatized nanotubes can be readily diluted by organic solvents, such as methanol, DMF, chloroform, and toluene, without precipitating the tubes and with little change in the electronic spectrum of the diluted solutions. Similar optical behavior was reported for SWNT−aniline solutions.[34] Upon dilution with acetone, however, a new peak at 330 nm is observed, which could be indicative of the presence of charge-transfer phenomenon in the adduct.

In general, the near-IR of dried, commercially available SWNTs in air show three characteristic optical absorptions at 0.67, 1.3, and 1.9 eV (approximately at 5400, 10 000, and 16 000 cm^{-1}, respectively), which can be attributed to optical transitions between van Hove singularities of the density of electronic states of these tubes; the first two transitions are assigned to semiconducting tubes, whereas the feature at 1.9 eV can be attributed to the first pair of such singularities in metallic tubes.[35] The observed peaks are due to overlapping van Hove transitions from all nanotube sizes that are present.

The presence of bands in the near-IR spectra of our functionalized nanotubes (Figure 6) indicates that the electronic structure of the tubes is preserved,[7,36] suggestive of the fact that the tubes are functionalized through coordinative attachment through dangling carboxyl and possibly alcoholic groups. This thus precludes coordination across electron-deficient double bonds, as observed[37] in, for example, $(C_2F_4)RhCl(PPh_3)_2$. At the same time, the large number of transitions observed also implies a broad-diameter distribution of tubes in the sample. The NIR spectra presented are shown with the regions of strong solvent absorbance omitted.[14] The spectrum from the functionalized adduct shows some clear differences from that of the raw nanotube sample.

Of particular significance is the presence of substructure and resolution of some of these peaks in the adduct spectrum, where only broad, unresolved humps had been seen for the raw, underivatized nanotubes. Because the width of the features in the NIR spectrum originates from the overlap of transitions from tubes of different diameters and helicities, the greater spectral resolution of peaks observed suggests that certain discrete diameter distributions of nanotubes may be preferentially solubilized.[14,38] In other words, there is evidence of a degree of

(33) Riggs, J. E.; Guo, Z.; Carroll, D. L.; Sun, Y. *J. Am. Chem. Soc.* **2000**, *122*, 5879.
(34) Sun, Y.; Wilson, S. R.; Schuster, D. I. *J. Am. Chem. Soc.* **2001**, *123*, 5348.
(35) Kavan, L.; Rupta, P.; Dunsch, L. *Chem. Phys. Lett.* **2000**, *328*, 363.
(36) Bahr, J. L.; Tour, J. M. *Chem. Mater.* **2001**, *13*, 3823.
(37) Hitchcock, P. B.; Mcpartlin, M.; Mason, R. *Chem. Commun.* **1969**, 1367.
(38) Jost, O.; Gorbunov, A. A.; Pompe, W.; Pickler, T.; Friedlein, R.; Kupfer, M.; Reibold, M.; Bauer, H.-D.; Dunsch, L.; Golden, M. S.; Fink, J. *Appl. Phys. Lett.* **1999**, *75*, 2217.

size and diameter selectivity, associated with the derivatization reaction and accompanying solubilization process.

As justification, spectra for two different concentrations of the adduct are shown in Figure 6; it is clear that the peak positions are not significantly affected by dilution. The major bands observed correspond to S_{11} and S_{22}, the transitions between the first and second pairs of singularities for the semiconducting tubes. The band at 5404 cm^{-1} (0.67 eV) is consistent with that of transitions observed for tubes with calculated diameters close to 1.3 nm.[39] Bands are also noted at 5968 and 6614 cm^{-1} (0.74 and 0.82 eV), which correspond to S_{11} transitions of tubes of 1.2 and 0.84 nm diameter, respectively. The corresponding S_{22} transitions are located at 10565, 7178−7340, and around 8146 cm^{-1} (1.31, 0.89−0.91, and around 1.01 eV), respectively. The S_{22} transitions in particular are shifted to slightly higher energy in the adduct and show greater resolution. Since the interband transition energy is inversely proportional to the tube diameter,[4,40,41] these data are indicative of preferential derivatization and dissolution of smaller-diameter tubes. The other implication is that the functionalization reaction may have the effect of slightly narrowing down the overall distribution of diameters in the sample, namely by skewing it toward smaller tubes, which would also lead to the higher spectral resolution observed. A doping-related upshift cannot be ruled out; however, charge transfer would be expected to have a greater effect on the S_{11} transitions.

Whereas interband transitions of metallic tubes are expected to lie in the 570−750-nm region and the corresponding UV−visible spectra of our functionalized tubes are similarly featureless in this region, such featureless electronic spectra have also been noted for functionalized metallic tubes in the past.[12,24,34] In fact, recent studies suggest perturbations, such as cutting, oxidizing, bending, and mechanically distorting nanotube bundles, can affect the electronic properties of these structures; the metallic nature of some individual SWNTs are particularly sensitive to such processing.[42] Hence, due to the chemical manipulation of the tubes in these experiments, it is likely that a similar phenomenon is responsible for the lack of apparent metallic features in our electronic spectra. Thus, to demonstrate the presence of "metallicity" in our adducts, we obtained fluorescence data on these structures.

Strong luminescence at room temperature has been previously detected in nanotube solutions,[33,43] and in these systems, the origin of this luminescence has been tentatively attributed to the existence of extensive conjugated electronic structures and the excitation-energy trapping associated with defects in the nanotubes. Our luminescence studies (Figure 7a) in DMSO indicated that the emission spectrum is strongly dependent on excitation wavelength, which is indicative of the presence of a large number of emitters and absorbers.[33] In fact, depending on the excitation wavelength used, two distinct classes of

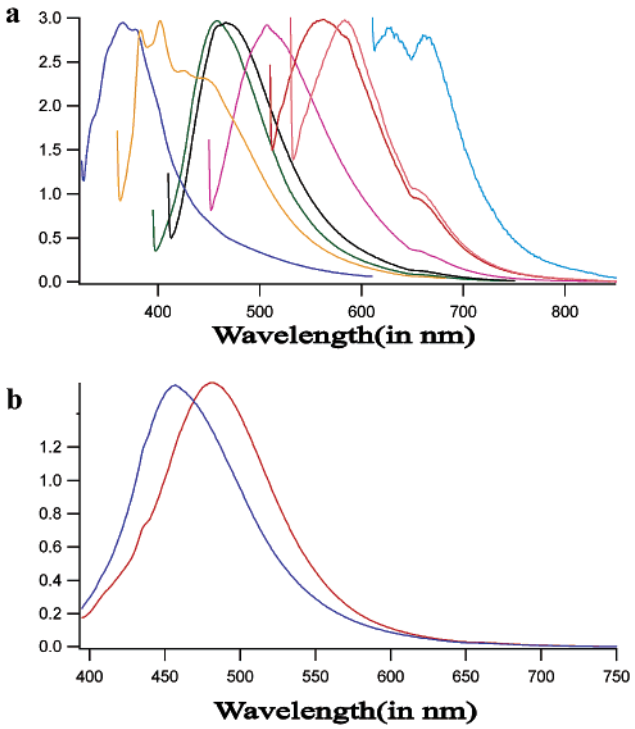

Figure 7. (a). Fluorescence emission spectra of functionalized nanotubes in DMSO solution upon excitation at 315, 350, 385, 400, 440, 500, 520, and 600 nm (from left to right), respectively. Note the excitation wavelength dependence of the emission maxima. Emission spectra show fine structure on excitation <385 nm. The emission peaks and presence of shoulders in the band in the 600−700-nm region correspond to the first emission band of metallic SWNTs. (b). Emission spectra upon excitation at 385 nm of a functionalized SWNT−Wilkinson's complex adduct solution in DMSO, diluted with acetone (blue) and methanol (red).

emitting species can be differentiated. One class can be probed upon excitation over a wide number of wavelengths in the range from 315 to 720 nm, corresponding to the presence of solubilized nanotube moieties. The emission spectra also contain a number of peaks of varying intensity in the 600−750 nm region, which likely originate from the first emission band of metallic SWNTs (M_{11} transitions).[44] The second class of emitters appears to be derived from the attached metal-containing complexes, more specifically the Rh species, which emit strongly upon excitation at around 350 nm. Emission spectra in this region show structure, which can be attributed to a superposition of emission from excitable Rh species onto the broader, almost Gaussian nanotube emission spectra.

As with other reports,[43] it seems likely that functionalization facilitates the manifestation of the intrinsic luminescence, emanating from these tubes, through dispersion of these nanotubes as well as trapping of the excitation energy on the nanotube surface itself. The slow motion of the tubes in solution suggests that this energy is not lost rapidly, and thus, the observed quenching and corresponding deactivation rate through molecular motion is slower.[34] Furthermore, the emission spectrum upon excitation at 385 nm (Figure 7b) shows a red-shift of the emission maximum from 457 nm in the acetone-diluted solution to 483 nm for the MeOH-diluted solution. Such an observed shift with increasing solvent polarity corroborates

(39) Hamon, M. A.; Itkis, M. E.; Niyogi, S.; Alvaraez, T.; Kuper, C.; Menon, M.; Haddon, R. C. *J. Am. Chem. Soc.* **2001**, *123*, 11292.
(40) Wildoer, J. W. G.; Venema, L. C.; Rinzler, A. G.; Smalley, R. E.; Dekker, C. *Nature* **1998**, *391*, 59.
(41) Kataura, H.; Kumazawa, Y.; Maniwa, Y.; Umezu, I.; Suzuki, S.; Ohtsuka, Y.; Achiba, Y. *Synth. Met.* **1999**, *103*, 2555.
(42) Goze Bac, C.; Latil, S.; Vaccarini, L.; Bernier, P.; Gaveau, P.; Tahir, S.; Micholet, V.; Aznar, R.; Rubio, A.; Metenier, K.; Beguin, F. *Phys. Rev. B* **2001**, *63*, 100302.
(43) Sun, Y.-P.; Zhou, B.; Henbest, K.; Fu, K.; Huang, W.; Lin, Y.; Taylor, S.; Carroll, D. L. *Chem. Phys. Lett.* **2002**, *351*, 349.
(44) Zhao, B.; Hu, H.; Niyogi, S.; Itkis, M. E.; Hamon, M. A.; Bhowmik, P.; Meir, M. S.; Haddon, R. C. *J. Am. Chem. Soc.* **2001**, *123*, 11673.

the presence of charge separation in the excited state in the SWNT−Wilkinson's adduct.[34,45]

Catalysis. An important consideration for the design of these adducts in particular has been their practical utility and efficiency in catalyzing chemical reactions. SWNTs have been used in the past as supports in heterogeneous catalysis.[46,47] In this study, the functionalized SWNT−Wilkinson's complex adducts have been found to catalyze the hydrogenation of cyclohexene to cyclohexane at room temperature. To the best of our knowledge, this represents the first example of a homogeneous catalysis reaction demonstrated using a nanotube support. This is significant because in more sophisticated reactions, the metal−support interactions in these functionalized nanotube adducts may provide a means of controlling the selectivity (such as the geometry and potentially, even the chirality) of the resultant product distribution. We are currently investigating and optimizing the kinetics of catalysis mediated by functionalized nanotube adducts.

Conclusions

Functionalization of oxidized SWNTs with Wilkinson's complex renders them soluble and stable in a variety of different organic solvents, thereby enabling further exploitation of their solution chemistry. The derivatization reaction occurs through the creation of a Rh metal−oxygen bond and results in exfoliation of larger nanotube bundles, creating an increased distribution of smaller-diameter tubes. Moreover, as the tubes are readily recoverable from solution, this finding has significant scientific and economic implications for nanotubes as reusable catalyst supports, particularly for expensive catalyst materials. We have been able to show the catalytic properties and reactivity of our synthesized complexes with respect to the hydrogenation of alkenes.

We expect similar types of nanotube coordination chemistry to be seen with other molecular complexes. Indeed, molecular metal complexation with nanotubes may not only provide the basis for site-selective nanochemistry applications but also enable a means of altering the known electronic and mechanical properties of SWNTs in a controllable manner. Because our studies also show the potential for novel charge-transfer characteristics in these functionalized materials, the development and understanding of these derivatized structures have implications for molecular electronics and photocatalysis as well as for scanning probe microscopy with functionalized tips.

Acknowledgment. We acknowledge support of this work through startup funds provided by the State University of New York at Stony Brook as well as Brookhaven National Laboratory. Acknowledgment is also made to the donors of the Petroleum Research Fund, administered by the American Chemical Society, for support of this research. Sigma Xi is also acknowledged for a Grant-in-Aid of Research. We also thank Dr. James Marecek and Dr. James Quinn for their guidance with the NMR and SEM/TEM work, respectively, as well as Ad Boyer and Ed Oliver (ThermoNicolet) who aided us with IR analyses. Kent Witter and Mark Wall (Jobin Yvon Spex) are acknowledged for their work with the fluorescence results.

JA026487O

(45) Hush, N. S.; Reimers, J. R. *Coord. Chem. Rev.* **1998**, *177*, 37.
(46) Planeix, J. M.; Coustel, N.; Coq, B.; Brotons, V.; Kumbhar, P. S.; Dutartre, R.; Geneste, P.; Bernier, P.; Ajayan, P. M. *J. Am. Chem. Soc.* **1994**, *116*, 7935.
(47) Lordi, V.; Yao, N.; Wei, J. *Chem. Mater.* **2001**, *13*, 733.